INTERNATIONAL JOURNAL OF CIRCUITS, SYSTEMS AND SIGNAL PROCESSING
DOI: 10.46300/9106.2023.17.17 Volume 17, 2023

DTC-SVM of sensorless five-phase induction machine using extended Kalman filter

Elakhdar Benyoussef, Said Barkat
Department of Electrical Engineering, University of Kasdi Merbah, Ouargla 30000, BP. 511 Algeria,

Received: September 5, 2022. Revised: February 4, 2023. Accepted: February 24, 2023. Published: March 13, 2023.

Abstract—This work relates to the study of direct torque control based on space vector modulation applied on five-phase induction machine. It is well established that the conventional direct torque control using hysteresis comparators suffers from high torque ripples and variable switching frequency. The most common solution to those problems is the use of space vector modulation. In the other hand, this paper aims also to design an extended Kalman filter observer for speed/flux estimation, which improves not only the control performances by using a sensorless algorithm but also can lower the cost and increase the reliability of the system. Both theoretical principle and simulation results of the sensorless control method of multiphase drive will be conducted to verify the effectiveness of the proposed control approach.

Keywords—Five-phase induction machine, five-phase inverter, DTC, SVM, extended Kalman Filter.

I. Introduction

VRIABLE speed electric drives are commonly based on three-phase machines. However, since the variable speed AC drives require a power electronic converter for their supply, the number of machine phases is essentially not limited [1]. Applications such as marine electric propulsion, electric vehicles, hybrid electric vehicles, electric aircraft, and locomotive traction are the main users of multiphase machines [2].

Actually, the multiphase machines have led to an increase in the interest in AC drive applications, since they offer some inherent advantages over their three-phase counterpart. These advantages include the ability to reduce the amplitude and to increase the frequency of torque pulsations by reducing the rotor harmonic current losses and lowering the DC-link current harmonics. In addition, owing to their redundant structure, multiphase machines improve the drives reliability [3].

In order to get smooth operation of the multiphase drives the multiphase machine has to be supplied with multiphase inverter. The use of multiphase inverters together with multiphase AC machines similarly has been recognized as a viable approach to obtain high power ratings with current limited devices [4].

Direct torque control has developed in past two decades and it is recognized as a powerful control method for motor drives with very simple implementation. DTC has been recently applied in multi–phase drives [5], [6] due to its multiple advantages including low machine parameters dependence and fast dynamic torque response [7].

However, the main drawbacks of this method are the high level of torque ripples and variable inverter switching frequency [6]. The solution to handle these problems is through using DTC scheme based on space vector modulation (DTC-SVM) [8]. Since, SVM technique generates a reference stator voltage vector with a constant frequency at every sampling time the inverter produces a voltage vector in any direction of variable magnitude, allowing a smooth torque change.

For many reasons, mainly for cost reduction and reliability increase, mechanical sensorless control of electrical drives has attracted the attention of researchers as well as many large manufacturers [9]; mechanical sensors are to be replaced by algorithms that estimate the rotor speed and position, based on electrical sensors measurement.

In order to reduce the number of sensors and consequently lowering the cost of control system, several speed sensorless control schemes have been suggested in literature [10] [11]. One of the most credible estimation methods is the extended Kalman filter (EKF), which is widely applied for drives sensorless control approaches even with multiphase machines [12]. The EKF is a recursive optimum stochastic state estimator. Therefore, model uncertainties and nonlinearities inherent in multiphase machines are well suited to the stochastic nature of EKF.

This paper is devoted to DTC-SVM of sensorless five-phase induction machine (FPIM) using extended Kalman filter (EKF) observer. The obtained results are compared to conventional DTC.

The present paper is organized as follows. In Section II, the (FPIM) model is reported. In Section III, details about SVM algorithm for five-phase inverter are given. In Section IV, the conventional DTC strategy is applied to get decoupled control of the stator flux and electromagnetic torque. Next, a brief introduction on the EKF algorithm is presented in Section V. Section VI introduces the DTC-SVM approach. Section VII is

devoted to the comparative study between DTC and DTC-SVM of sensorless (FPIM). Finally, conclusions are drawn in the last Section.

II. Modeling of Five-Phase Induction Machine

FPIM is characterized by a spatial displacement between phases of 72 degrees [5]. For the sake of generality, the rotor winding is treated as an equivalent five-phase winding of the same properties as the stator winding. To model the FPIM, the following assumptions are taken into account:

- Five phases of the machine are regularly shifted by 2π/5;
- Magnetic saturation is neglected;
- The stator phases are star connected.

Under balanced conditions, the voltage equations of a FPIM are given by:

$$\begin{cases} v_s = R_s i_s + \dfrac{d\phi_s}{dt} \\ 0 = R_r i_r + \dfrac{d\phi_r}{dt} \end{cases} \quad (1)$$

With:

$v_s = [v_{sa} \quad v_{sb} \quad v_{sc} \quad v_{sd} \quad v_{se}]^T$: is the stator voltage vector;

$i_s = [i_{sa} \quad i_{sb} \quad i_{sc} \quad i_{sd} \quad i_{se}]^T$: is the stator current vector;

$i_r = [i_{ra} \quad i_{rb} \quad i_{rc} \quad i_{rd} \quad i_{re}]^T$: is the rotor current vector;

$\phi_s = [\phi_{sa} \quad \phi_{sb} \quad \phi_{sc} \quad \phi_{sd} \quad \phi_{se}]^T$: is the stator flux vector;

$\phi_r = [\phi_{ra} \quad \phi_{rb} \quad \phi_{rc} \quad \phi_{rd} \quad \phi_{re}]^T$: is the rotor flux vector.

The model can be presented in the stationary reference, in which two orthogonal frames called α-β and z_1-z_2 are used, where the α-β components are responsible for developing the fluxes and the torque, while the remaining z_1-z_2 components generate the machine losses [7].

The original five-dimensional stator system can be decomposed into three-dimensional decoupled subsystems using the following transformation:

$$\left[X_\alpha \quad X_\beta \quad X_{z1} \quad X_{z2} \quad X_o\right]^T = [A][X] \quad (2)$$

with

$$[X] = [X_a \quad X_b \quad X_c \quad X_d \quad X_e]^T$$

where X can be used to stand for current vectors (i_s, i_r), flux vectors (ϕ_s, ϕ_r) or voltage vectors (v_s, v_r).

The matrix A is given by:

$$[A] = \sqrt{\frac{2}{5}} \begin{bmatrix} \cos(0) & \cos\left(\frac{2\pi}{5}\right) & \cos\left(\frac{4\pi}{5}\right) & \cos\left(\frac{6\pi}{5}\right) & \cos\left(\frac{8\pi}{5}\right) \\ \sin(0) & \sin\left(\frac{2\pi}{5}\right) & \sin\left(\frac{4\pi}{5}\right) & \sin\left(\frac{6\pi}{5}\right) & \sin\left(\frac{8\pi}{5}\right) \\ \cos(0) & \cos\left(\frac{4\pi}{5}\right) & \cos\left(\frac{8\pi}{5}\right) & \cos\left(\frac{12\pi}{5}\right) & \cos\left(\frac{16\pi}{5}\right) \\ \sin(0) & \sin\left(\frac{4\pi}{5}\right) & \sin\left(\frac{8\pi}{5}\right) & \sin\left(\frac{12\pi}{5}\right) & \sin\left(\frac{16\pi}{5}\right) \\ \frac{1}{\sqrt{2}} & \frac{1}{\sqrt{2}} & \frac{1}{\sqrt{2}} & \frac{1}{\sqrt{2}} & \frac{1}{\sqrt{2}} \end{bmatrix} \quad (3)$$

The stator voltage equations of the FPIM can be obtained in the stationary reference frame as follows:

$$\begin{cases} v_{s\alpha} = R_s i_{s\alpha} + \dfrac{d\phi_{s\alpha}}{dt} \\ v_{s\beta} = R_s i_{s\beta} + \dfrac{d\phi_{s\beta}}{dt} \\ v_{sz1} = R_s i_{sz1} + \dfrac{d\phi_{sz1}}{dt} \\ v_{sz2} = R_s i_{sz2} + \dfrac{d\phi_{sz2}}{dt} \end{cases} \quad (4)$$

with $v_{s\alpha}$, $v_{s\beta}$ are the α-β components of stator voltage, v_{sz1}, v_{sz2} are the z_1-z_2 components of stator voltage, $i_{s\alpha}$, $i_{s\beta}$ are the α-β components of stator current and $i_{s\alpha}$, $i_{s\beta}$ are the z_1-z_2 components of stator current.

The rotor voltage equations of the FPIM can be obtained in the stationary reference frame as follows:

$$\begin{cases} 0 = R_r i_{r\alpha} + \dfrac{d\phi_{r\alpha}}{dt} - \omega\phi_{r\beta} \\ 0 = R_r i_{r\beta} + \dfrac{d\phi_{r\beta}}{dt} + \omega\phi_{r\alpha} \\ 0 = R_r i_{rz1} + \dfrac{d\phi_{rz1}}{dt} \\ 0 = R_r i_{rz2} + \dfrac{d\phi_{rz2}}{dt} \end{cases} \quad (5)$$

with $i_{r\alpha}$, $i_{r\beta}$ are the α-β components of rotor current and i_{rz1}, i_{rz2} are the z_1-z_2 components of rotor current.

The stator and rotor flux linkages of these subspaces are:

$$\begin{cases} \phi_{s\alpha} = L_s i_{s\alpha} + M i_{r\alpha} \\ \phi_{s\beta} = L_s i_{s\beta} + M i_{r\beta} \\ \phi_{r\alpha} = L_r i_{r\alpha} + M i_{s\alpha} \\ \phi_{r\beta} = L_r i_{r\beta} + M i_{s\beta} \\ \phi_{sz1} = l_s i_{sz1} \\ \phi_{sz2} = l_s i_{sz2} \\ \phi_{rz1} = l_r i_{rz1} \\ \phi_{rz2} = l_r i_{rz2} \end{cases} \quad (6)$$

with $\phi_{s\alpha}$, $\phi_{s\beta}$ are the α-β components of stator flux, $\phi_{r\alpha}$, $\phi_{r\beta}$ are the α-β components of rotor flux, ϕ_{sz1}, ϕ_{sz2} are the z_1-z_2 components of stator flux, and ϕ_{rz1}, ϕ_{rz2} are the z_1-z_2 components of rotor flux.

Since the (α, β) machine model is similar to the three-phase machine model in the stationary reference frame, the electromagnetic torque expression can be easily deduced as:

$$T_{em} = p\left(\phi_{s\alpha} i_{s\beta} - \phi_{s\beta} i_{s\alpha}\right) \quad (7)$$

In order to transform variables in the stator flux reference frame α-β to the stator flux reference frame *x*-*y*, the following rotation transformation is adopted:

$$\left[P(\theta_s)\right] = \begin{bmatrix} \cos(\theta_s) & -\sin(\theta_s) \\ \sin(\theta_s) & \cos(\theta_s) \end{bmatrix} \quad (8)$$

where θ_s is the stator flux angle.

In the *x*-*y* stator flux reference frame, the voltage equation becomes:

$$\begin{cases} v_{sx} = R_s i_{sx} + \dfrac{d\phi_{sx}}{dt} - \omega\phi_{sy} \\ v_{sy} = R_s i_{sy} + \dfrac{d\phi_{sy}}{dt} + \omega\phi_{sx} \end{cases} \quad (9)$$

with v_{sx}, v_{sy} are the *x*-*y* components of stator voltage, i_{sx}, i_{sy} are the *x*-*y* components of stator current, and ϕ_{sx}, ϕ_{sy} are the *x*-*y* components of stator flux.

The electromagnetic torque takes the following form:

$$T_{em} = p\left(\phi_{sx} i_{sy} - \phi_{sy} i_{sx}\right) \quad (10)$$

The mechanical equation is given by:

$$J\frac{d\Omega}{dt} = T_{em} - T_L - f\Omega \quad (11)$$

with T_{em} is the electromagnetic torque, T_L is the load torque, Ω is the rotor speed, and f is the friction coefficient.

III. Five-Phase Two-Level Space Vector Modulation

Two-level five-phase inverter consists of ten pairs of transistors-diodes as shown in Fig. 1. The phase voltage of each phase is entirely defined by the state of the two transistors constituting each arm. In the five-phase inverter, each leg switching function that is called S_x (x=*a*, *b*, *c*, *d*) and can take either 1 or 0 value based on the state of the upper or lower switch. If the upper switch is ON then the switching function takes a value of 1 else 0.

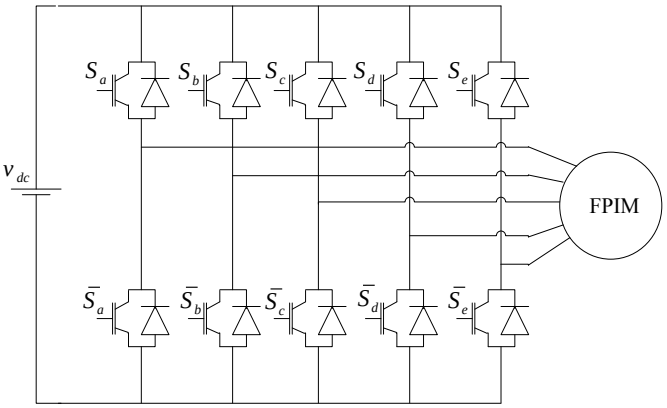

Fig. 1 schematic diagram of a two-level five-phase inverter.

The phase voltages of five-phase inverter are given by:

$$\begin{pmatrix} v_{sa} \\ v_{sb} \\ v_{sc} \\ v_{sd} \\ v_{se} \end{pmatrix} = \frac{v_{dc}}{5} \begin{pmatrix} 4 & -1 & -1 & -1 & -1 \\ -1 & 4 & -1 & -1 & -1 \\ -1 & -1 & 4 & -1 & -1 \\ -1 & -1 & -1 & 4 & -1 \\ -1 & -1 & -1 & -1 & 4 \end{pmatrix} \begin{pmatrix} S_a \\ S_b \\ S_c \\ S_d \\ S_e \end{pmatrix} \quad (12)$$

Thirty two switching combinations can be considered for a five-phase inverter: two zero voltage vectors and thirty active space voltage vectors. In a five-phase inverter, all the five-phase variables can be represented in α-β subspaces. The 32 space voltage vectors are composed of three sets of different vector amplitudes and divide the switching plane pattern into ten sectors [10]. All output voltage vectors generated by five-phase voltage source inverter are presented in Fig. 2.

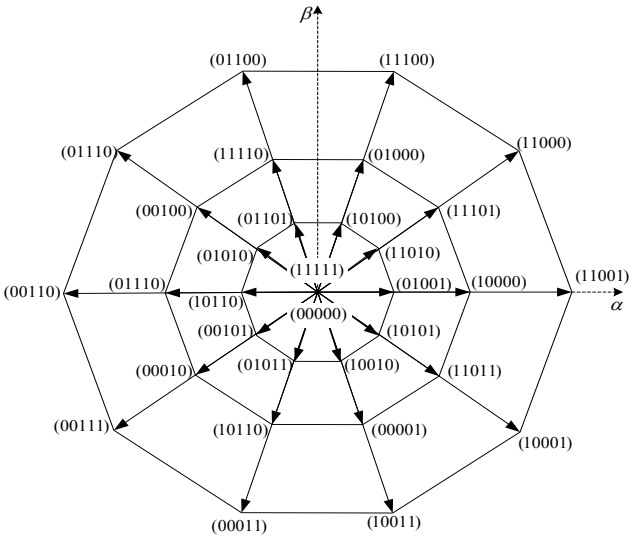

Fig. 2 space voltage vectors of a five-phase inverter in α-β plane.

In every sector, the reference voltage vector is synthesized by two adjacent active voltage vectors and one zero vector. For example, in the first sector, v_s^* is synthesized using v_0, v_1 and v_2 according to the following equation:

$$\begin{cases} v_s^* T_{sw} = t_o v_o + t_1 v_1 + t_2 v_2 \\ T_{sw} = t_o + t_1 + t_2 \\ v_s^* = v_{s\alpha}^* + j v_{s\beta}^* \end{cases} \quad (13)$$

where t_o, t_1, t_2 are the application times of the space voltage vectors v_o, v_1, v_2, respectively during a switching period T_{sw}.

Fig. 3 presents the projection of the reference voltage vector in sector 1.

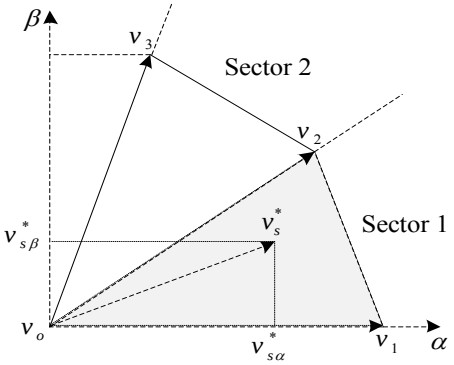

Fig. 3 projection of the reference voltage vector in sector 1.

From Fig. 3, the space voltage v_0, v_1 and v_2 can be expressed as:

$$\begin{cases} v_o = 0 \\ v_1 = \sqrt{\frac{2}{5}} v_{dc} \\ v_2 = \sqrt{\frac{2}{5}} v_{dc} \left(\cos(2\pi/5) + j \sin(2\pi/5) \right) \end{cases} \quad (14)$$

After projection, and using (14) it is possible to get:

$$\begin{cases} v_{s\alpha}^* = t_1 \sqrt{\frac{2}{5}} v_{dc} + t_2 \sqrt{\frac{2}{5}} v_{dc} \cos(\pi/5) \\ v_{s\beta}^* = t_2 \sqrt{\frac{2}{5}} v_{dc} \sin(\pi/5) \end{cases} \quad (15)$$

The switching times applied for first sector are given by:

$$\begin{cases} t_1 = \sqrt{\frac{5}{2}} \frac{v_{s\alpha}^*}{v_{dc}} - \sqrt{\frac{5}{2}} \frac{\cos(\pi/5)}{v_{dc} \sin(\pi/5)} v_{s\beta}^* \\ t_2 = \sqrt{\frac{5}{2}} \frac{v_{s\beta}^*}{v_{dc} \sin(\pi/5)} \\ t_0 = T_{sw} - t_1 - t_2 \end{cases} \quad (16)$$

Fig. 4 illustrates the gates pulses generated in sector 1. It is about symmetrical signals that have the same states at the center and at the ends.

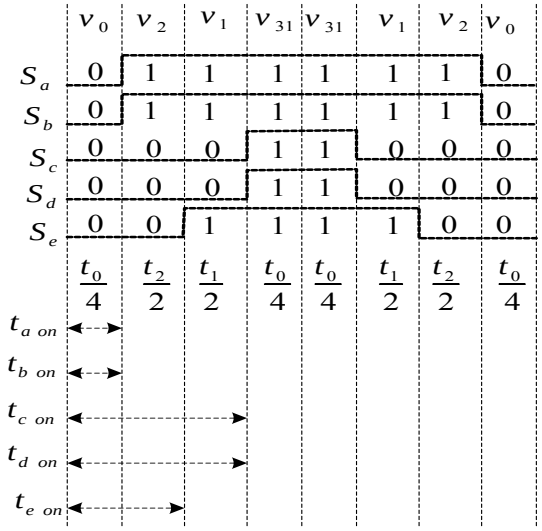

Fig. 4 examples of chronograms pulses of sector 1.

IV. Conventional Direct Torque Control

Fig. 5 represents the direct torque control scheme of sensorless FPIM.

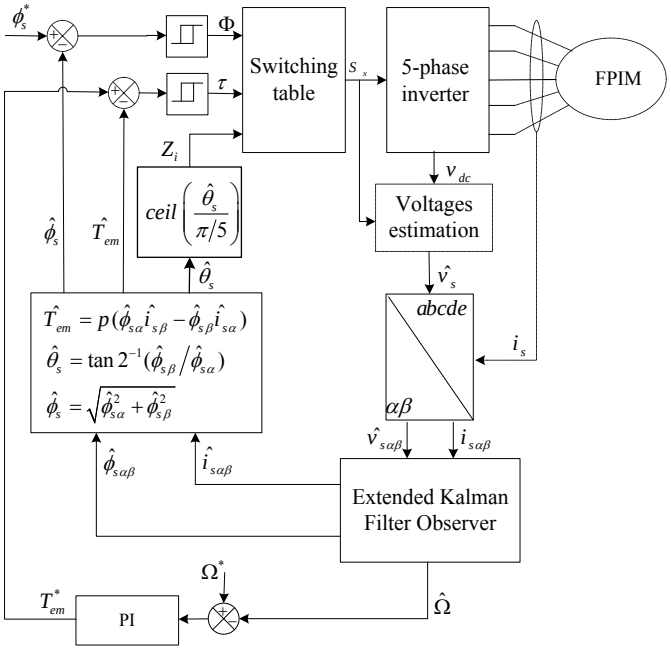

Fig. 5 DTC scheme for sensorless FPIM.

In Fig. 6, the vectors with maximum amplitude are named large vectors, the vectors with minimum amplitude are named small vectors, and vectors whose amplitude is larger than small vectors and smaller than large vector are named middle vectors.

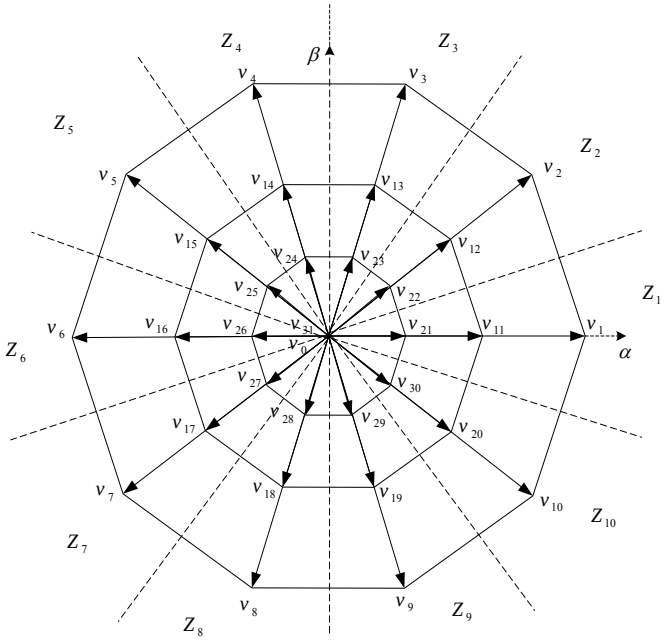

Fig. 6 switching states of the five-phase inverter in α-β plane.

In conventional DTC, the stator flux and electromagnetic torque are controlled by selecting directly the appropriate inverter switching states. The DTC scheme consists in torque and flux hysteresis bands, switching table, and flux and torque estimator [5].

The stator voltage components can also be estimated using the flowing equation:

$$\left[\hat{v}_{s\alpha} \quad \hat{v}_{s\beta}\right]^T = [A][\hat{v}_s] \tag{17}$$

with $\hat{v}_s = \left[\hat{v}_{sa} \quad \hat{v}_{sb} \quad \hat{v}_{sc} \quad \hat{v}_{sd} \quad \hat{v}_{se}\right]^T$ is given by (12).

The switching selection table for the conventional DTC for FPIM is given in Table 1.

Table 1. Switching table used in the conventional DTC (i=*1*, *2*, …, 10).

Φ	τ	Z_i
1	2	$v_{(i+1)}$
	1	$v_{(i+11)}$
	0	$v_{(i+20)}$
	-1	$v_{(i+19)}$
	-2	$v_{(i+29)}$
-1	2	$v_{(i+4)}$
	1	$v_{(i+14)}$
	0	$v_{(i+25)}$
	-1	$v_{(i+18)}$
	-2	$v_{(i+28)}$

V. Extended Kalman Filter Observer

The extended Kalman filter is basically a full order stochastic observer for recursive optimum state estimation of nonlinear dynamical systems in real time by using signals that are corrupted by noise; the noise source in EKF takes into account measurement and modeling inaccuracies [13].
The development of the Kalman filter is closely linked to the stochastic systems that can take the following form:

$$\begin{cases} \dot{x}(t) = Ax(t) + Bu(t) + w(t),\ x(t_o) = x_o \\ y(t) = Cx(t) + v(t) \end{cases} \tag{18}$$

where *w* and *v* are the system and measurement noises.

The extended Kalman filter implementation for the FPIM requires two basic steps:

- Continuous FPIM model,
- Discretization of the FPIM model.

A. Continuous FPIM Model

The model of the FPIM in the α-β reference can be written in the following from:

$$\begin{cases} \dot{x}(t) = Ax(t) + Bu(t) \\ y(t) = Cx(t) \end{cases} \tag{19}$$

with $x(t)=\begin{bmatrix} i_{s\alpha} & i_{s\beta} & \phi_{s\alpha} & \phi_{s\beta} & \Omega \end{bmatrix}^T$ is the state vector, $y=\begin{bmatrix} i_{s\alpha} & i_{s\beta} \end{bmatrix}^T$ is the output vector, $u=\begin{bmatrix} v_{s\alpha} & v_{s\beta} \end{bmatrix}^T$ is the input vector, and the system matrices are:

$$A=\begin{bmatrix} -\frac{R_t}{\sigma} & -p\Omega & -\frac{R_r}{\sigma} & -p\Omega\frac{L_r}{\sigma} & 0 \\ p\Omega & -\frac{R_t}{\sigma} & p\Omega\frac{L_r}{\sigma} & -\frac{R_r}{\sigma} & 0 \\ -R_s & 0 & 0 & 0 & 0 \\ 0 & -R_s & 0 & 0 & 0 \\ -\frac{p\phi_{s\beta}}{J} & \frac{p\phi_{s\alpha}}{J} & 0 & -\frac{f}{J} & 0 \end{bmatrix}, B=\begin{bmatrix} -\frac{L_r}{\sigma} & 0 & 0 \\ 0 & -\frac{L_r}{\sigma} & 0 \\ 1 & 0 & 0 \\ 0 & 1 & 0 \\ 0 & 0 & \frac{-1}{J} \end{bmatrix},$$

$$C=\begin{bmatrix} 1 & 0 & 0 & 0 & 0 \\ 0 & 1 & 0 & 0 & 0 \end{bmatrix}$$

where $R_t=-(R_sL_r+R_rL_s)$, $\delta=M^2-L_sL_r$

B. Discretization of the FPIM Model

The discrete time model is given by:

$$\begin{cases} x_{j(k+1)}=A_{jk}x_{jk}+B_{jk}u_{kj}+\omega_{jk} \\ y_{jk}=C_{jk}x_{jk}+v_{jk} \end{cases} \quad (20)$$

The discretization is performed using the following approximation:

$$\begin{cases} A_{jk}=e^{At}=I+AT_s \\ B_{jk}=\int_0^t e^{A\xi}Bd\xi=BT_s \\ C_{jk}=C \end{cases} \quad (21)$$

The matrix A_{jk}, B_{jk} and C_{jk} are given by:

$$A_{jk}=\begin{bmatrix} 1-\frac{T_sR_t}{\sigma} & -T_sp\Omega & -\frac{T_sR_r}{\sigma} & -p\Omega\frac{T_sL_r}{\sigma} & 0 \\ T_sp\Omega & 1-\frac{T_sR_t}{\sigma} & p\Omega\frac{T_sL_r}{\sigma} & \frac{T_sR_r}{\sigma} & 0 \\ -T_sR_s & 0 & 1 & 0 & 0 \\ 0 & -T_sR_s & 0 & 1 & 0 \\ -\frac{T_sp\phi_{s\beta}}{J} & \frac{T_sp\phi_{s\alpha}}{J} & 0 & -\frac{T_sf}{J} & 1 \end{bmatrix},$$

$$B_{jk}=\begin{bmatrix} -\frac{T_sL_r}{\sigma} & 0 & 0 \\ 0 & -\frac{T_sL_r}{\sigma} & 0 \\ T_s & 0 & 0 \\ 0 & T_s & 0 \\ 0 & 0 & \frac{-T_s}{J} \end{bmatrix}, C_{jk}=\begin{bmatrix} 1 & 0 & 0 & 0 & 0 \\ 0 & 1 & 0 & 0 & 0 \end{bmatrix}$$

Using equation (20), the rotor speeds and load torques can be estimated by the extended Kalman filter algorithm described as follows:

Sate prediction:

$$\hat{x}_{j(k+1/k)}=A_{jk}x_{j(k/k)}+B_{jk}u_{jk} \quad (22)$$

Estimation of the matrix of the covariance error:

$$\hat{P}_{j(k+1/k)}=A_{jk}P_{j(k/k)}A_{jk}^T+Q_j \quad (23)$$

Kalman coefficient update:

$$K_{j(k+1)}=\hat{P}_{j(k+1/k)}C_{jk}^T\left[C_{jk}\hat{P}_{j(k+1/k)}C_{jk}^T+R_j\right]^{-1} \quad (24)$$

State estimation:

$$\hat{x}_{j(k+1/k+1)}=\hat{x}_{j(k+1/k)}+K_{j(k+1)}\left(y_{j(k+1)}-C_{jk}\hat{x}_{j(k+1/k)}\right) \quad (25)$$

Covariance error matrix update:

$$\hat{P}_{j(k+1/k+1)}=\hat{P}_{j(k+1/k)}-K_{j(k+1)}C_{jk}\hat{P}_{j(k+1/k)} \quad (26)$$

where $\hat{x}$ is the system state, u_{jk} is the system input vector, y is the system output vector, P, Q and R are the covariance matrices, C is the transformation matrix.

The magnitude of stator flux can be estimated by:

$$\left|\hat{\phi}_s\right|=\sqrt{\hat{\phi}_{s\alpha}^2+\hat{\phi}_{s\beta}^2} \quad (27)$$

The stator flux angle is calculated by:

$$\hat{\theta}_s=\arctan\left(\frac{\hat{\phi}_{s\beta}}{\hat{\phi}_{s\alpha}}\right) \quad (28)$$

The electromagnetic torque can be estimated using estimated fluxes and measured currents as follows:

$$\hat{T}_{em}=p\left(\hat{\phi}_{s\alpha}i_{s\beta}-\hat{\phi}_{s\beta}i_{s\alpha}\right) \quad (29)$$

VI. DTC BASED ON SPACE VECTOR MODULATION STRATEGY

The block diagram of the DTC-SVM scheme of the sensorless FPIM is shown in Fig. 7. Two PI regulate flux and torque errors giving reference voltage vector in *x-y* coordinates. After transformation, the voltage vector in *α-β* coordinates is delivered to SVM block.

The basis of the DTC-SVM methodology is the generation, at each sampling period, of a required voltage space vector to compensate for the flux and torque errors using SVM [14]. The presented control strategy is based on simplified stator

voltage equations described in stator flux oriented x-y coordinates, in which the stator flux is along the *x*-axis, which results in $\phi_{ys} = 0$ and $\phi_{sx} = \phi_s$.

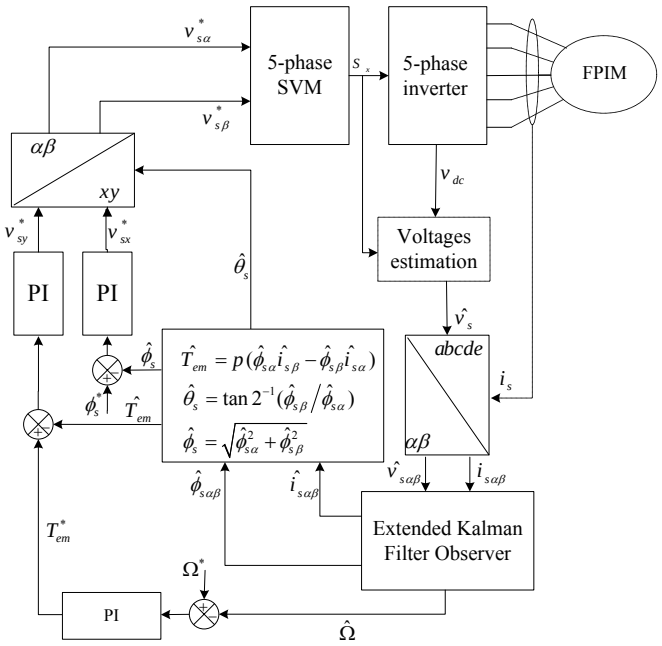

Fig. 7 DTC-SVM scheme for sensorless FPIM.

The components of stator voltage vector, given by (9), are simplified to:

$$\begin{cases} v_{sx} = R_s i_{sx} + \dfrac{d\phi_s}{dt} \\ v_{sy} = R_s i_{sy} + \omega_s \phi_s \end{cases} \tag{30}$$

The electromagnetic torque equation is reduced to:

$$T_{em} = p|\phi_s| i_{sy} \tag{31}$$

The first equation of (30) shows that the v_{sx} component has an influence only on the change of stator flux magnitude ϕ_s, and if the term $\omega_s \phi_s$ is decoupled the component v_{sy} can be used for torque adjustment.

So, the next step is to transform *x-y* reference voltage vector components to the stationary reference frame using the following transformation.

$$\begin{pmatrix} v_{s\alpha}^* \\ v_{s\beta}^* \end{pmatrix} = \left[P(\theta_s)\right]^{-1} \begin{pmatrix} v_{sx}^* \\ v_{sy}^* \end{pmatrix} \tag{32}$$

The stator flux and electromagnetic torque control loops for the DTC-SVM of FPIM in *x-y* reference are shows in Fig. 8.

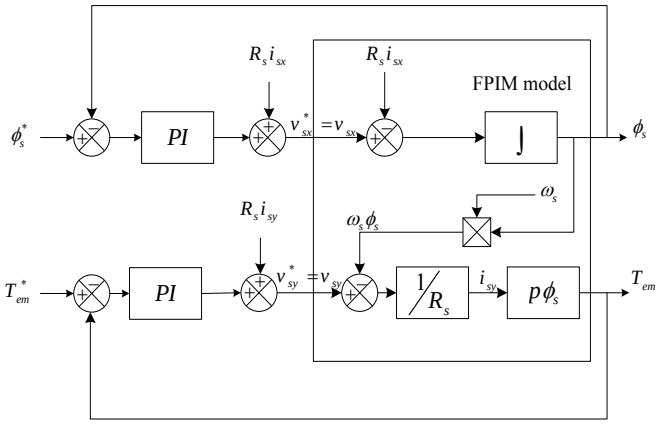

Fig. 8 stator flux and electromagnetic torque control loop with two *PI* controllers in *x-y* reference frame.

VII. Comparative Study between DTC and DTC-SVM

The obtained conventional DTC results are presented and compared with those obtained by DTC-SVM using the FPIM parameters given in the Appendix. The proposed control method has been tested under reversal speed condition whereas the machine is loaded at the beginning by a rated torque.

A. Dynamic performances during speed and load torque variations

To test the speed evolution, the FPIM is accelerate from standstill to reference speed *100rad/s* with a load variation of *8Nm* to *0Nm* at *1*s followed by a speed inversion from *100rad/s* to *-100*rd/s at *1.5*s. Indeed, Figs. 9 and 10 show the simulation results obtained using conventional DTC and DTC-SVM of sensorless FPIM, respectively.

Situation 1: Step change in load torque. Note that, both control approaches ensure good decoupling between stator flux linkage and electromagnetic torque. However the DTC based on SVM for the FPIM decreases considerably the torque ripples.

Situation 2: Step change in reference speed. Note that the control gives good quality results with the speed variation. The speed response is merged with the reference one and the flux is very similar to the nominal case. We can see also, that the DTC-SVM for FPIM decrease considerably the torque and flux ripples.

B. Dynamic performances during low speed operations

In order to verify the robustness of the proposed control using extended Kalman observer, a low speed test has been performed. The FPIM is accelerating from standstill to reference speed *10*rad/s. The system is started with full load torque *8*N.m, afterwards; the FPIM is accelerated again to reference speed *20*rad/s at time *0.4*s. Afterwards, a step variation on the load torque (T_L = 0N.m) is applied at time t=0.8s. Finally, it is decelerate to the reference speed *-10* rad/s at time *1.2*s.

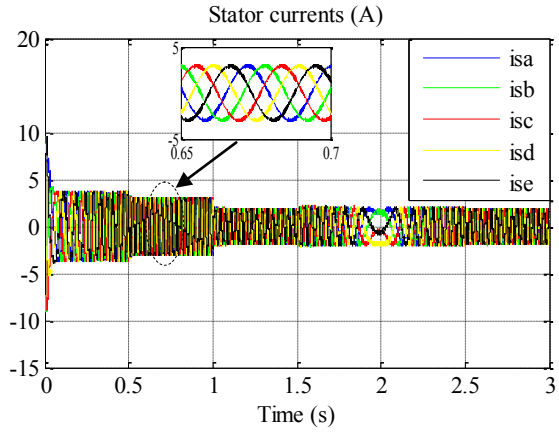

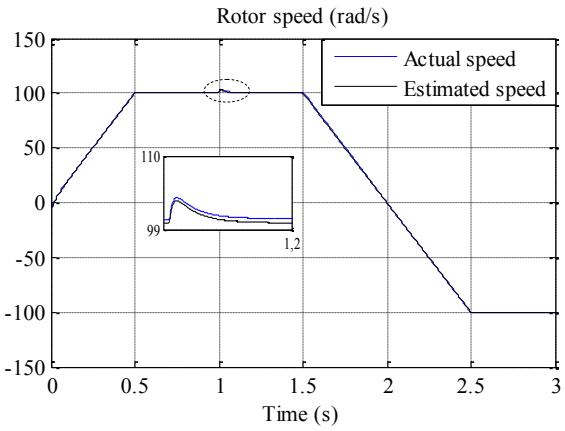

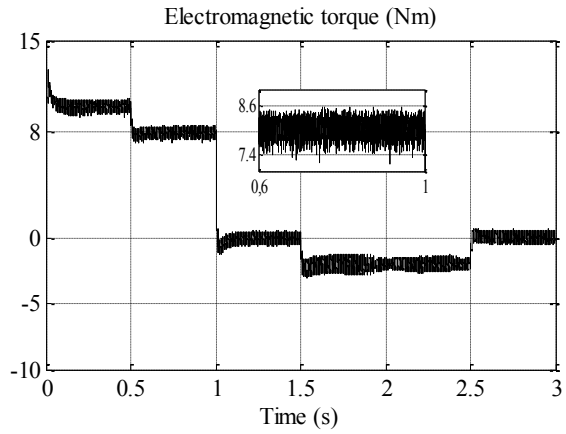

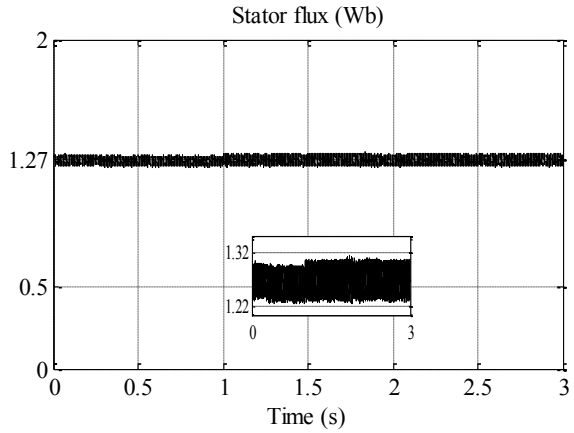

Fig. 9 dynamic responses of DTC for sensorless FPIM.

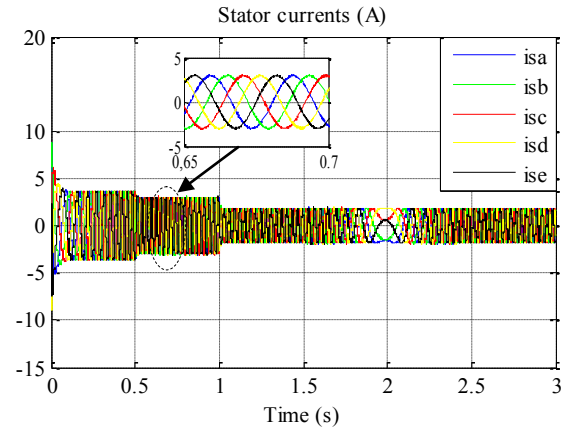

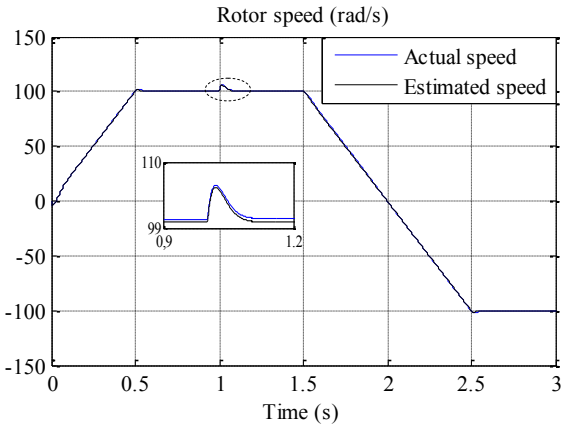

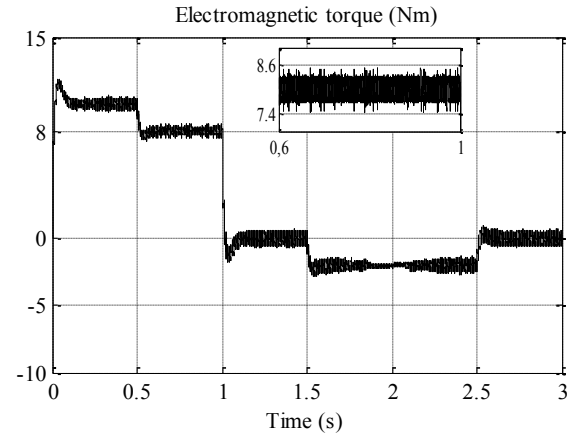

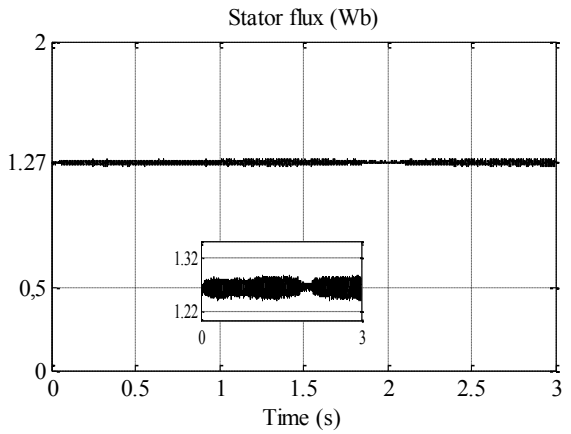

Fig. 10 dynamic responses of DTC-SVM for sensorless FPIM.

Fig. 11 shows the performances of the DTC-SVM for sensorless FPIM using extended Kalman observer under low speed operation. Simulation results show that the speed follows its reference value while the electromagnetic torque reaches slowly its reference value. Elimination of the load torque causes a slight variation in speed response. The speed controller intervenes to face this variation and ensures the system follows its suitable reference speed.

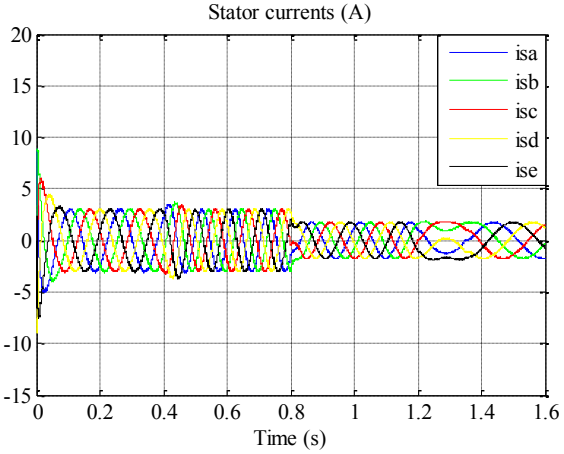

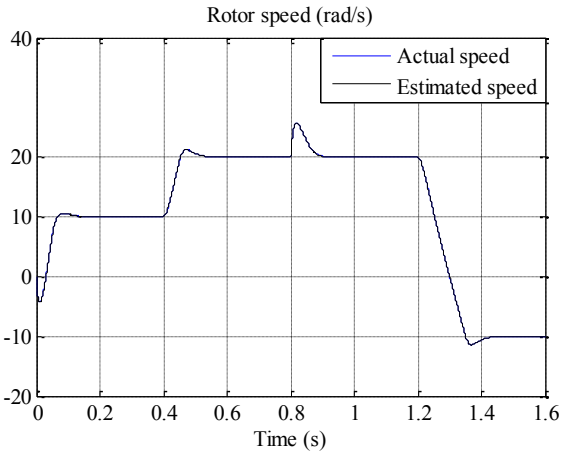

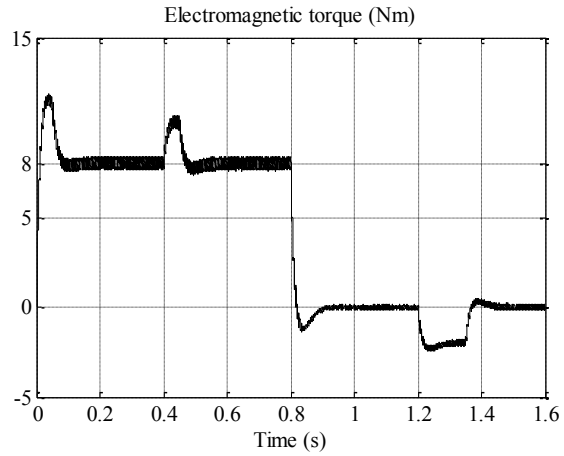

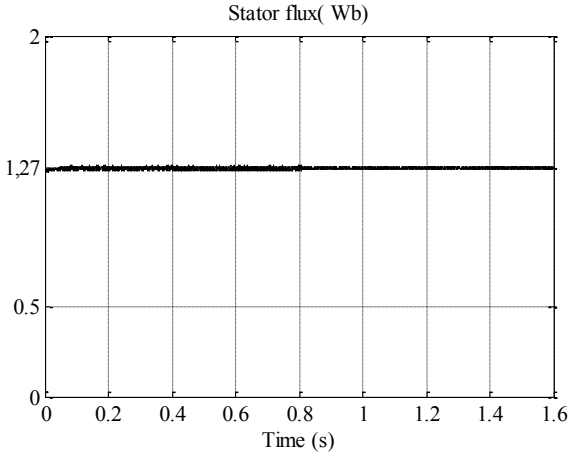

Fig. 11 dynamic responses of DTC-SVM for sensorless FPIM for low speed.

Moreover, the decoupling control between torque and stator flux is always confirmed. Note also that the sensorless controller is effective to drive the multiphase machine to track the speed reference even in low speed. Furthermore, the proposed observer is accurate and robust against load torque variation even at low speed operations.

VIII. Conclusion

In this paper, a DTC based on space vector modulation method applied on FPIM is presented and its merits over the conventional DTC approach are verified. Indeed, the simulation results confirm that the proposed DTC-SVM scheme achieves a fast torque response and low torque and flux ripples in comparison to the conventional DTC scheme. The decoupling between the flux and the torque is maintained, which confirms the good performances of the developed drive system. In addition, the proposed sensorless multiphase drive has a satisfactory dynamic response over a wide speed range.

Appendix

Table 2 FPIM parameters.

Quantity	Symbol	Value
Stator resistance	R_s	10 Ω
Rotor resistance	R_r	6.3 Ω
Stator inductance	L_s	0.46 H
Rotor inductance	L_r	0.46 H
Mutual inductance	M	0.42 H
Inertia moment	J	0.01 Nms^2/rad
Pair of pole	p	2
Rated flux	ϕ_{sn}	1.2705 Wb
Rated torque	T_n	8.33Nm
Rated speed	Ω_n	1500 *rpm*

REFERENCES

[1] S. Basak, C. Chakraborty, "Dual stator winding induction machine: problems, progress, and future scope," IEEE Transaction on Industrial Electronics, vol. 62 no. 7, pp. 4641-4652. 2015.

[2] K. Iffouzar, B. Amrouche, T. Cherif, M. Benkhoris, D. Aouzellag, K. Ghedamsi, "Improved direct field oriented control of multiphase induction motor used in hybrid electric vehicle application," International Journal of Hydrogen Energy, vol. 42, no. 30, pp. 19296-19308, 2017.

[3] C. Shantanu, C. Saibal, "A novel speed sensor-less vector control of dual stator induction machine with space vector based advanced 9-zone hybrid PWM for grid connected wind energy generation system," Electric Power Systems Research, vol. 163, pp. 174-195, 2018.

[4] T. Zoheir, O. Malik, A. Eltamaly, "Fuzzy logic based speed control of indirect field oriented controlled Double Star Induction Motors connected in parallel to a single six-phase inverter supply," Electric Power Systems Research, vol. 134, pp. 126-133, 2016.

[5] Y. Tatte, M. Aware, "Direct torque control of five-phase induction motor with common-mode voltage and current harmonics reduction," IEEE Journal of Transaction on Power Electronics, vol. 32, no. 11, pp. 1-11, 2016.

[6] V. Talaeizadeh, R. Kianinezhad, S. Seyfossadat, H. Shayanfar, "Direct torque control of six-phase induction motors using three-phase matrix converter," Energy Conversion and Management, vol. 51, pp. 2482-2491, 2010.

[7] R. Sundram, B. Auzani, L. Logan, A. Mohamed, A. Kasrul, "Improved performance of DTC for 5-phase induction machine using open-end topology," IEEE Energy Conversion, Conference on Johor Bahru, Malaysia, 2014.

[8] Z. Zhifeng, T. Renyuan, B. Baodong, X. Dexin, "Novel direct torque control based on space vector modulation with adaptive stator flux observer for induction motors," IEEE Transaction on Magnetics, vol. 46, no. 8, pp. 3133-3136, 2010.

[9] Z. Ying, M. Cheng, H. Wei, Z. Bangfu, "Sensorless control strategy of electrical variable transmission machines for wind energy conversion systems," IEEE Transactions on Magnetics, vol. 49, no. 7, pp. 3383-3386, 2013.

[10] H. Echeikh, R. Trabelsi, A. Iqbal, M. Mimouni, "Adaptive direct torque control using Luenberger-sliding mode observer for online stator resistance estimation for five-phase induction motor drives," Journal of Electrical Engineering, vol. 100, no. 3, pp. 1639-1649, 2017.

[11] I. Benlaloui, S. Drid, L. Alaoui, M. Ourgiali, "Implementation of a new MRAS speed sensorless vector control of induction machine," IEEE Transactions on Energy Conversion, vol. 30, no. 2, pp. 588-595, 2015.

[12] M. Barut, R. Demir, E. Zerdali, R. Inan, "Real-time implementation of bi input extended Kalman filter based estimator for speed sensorless control of induction motors," IEEE Transaction on Industrial Electronics, vol. 59, no. 11, pp. 4197-4206, 2012.

[13] M. Merzoug, H. Benalla, H. Naceri, "Speed estimation using extended filter Kalman for the direct torque controlled permanent magnet synchronous motor (PMSM)," IEEE, International Conference on Computer and Electrical Engineering, pp. 124-127, 2009.

[14] M. Jones, I. Satiawan, N. Bodo, E. Levi, "A dual five-phase space vector modulation algorithm based on the decomposition method," IEEE Transactions on Industry Application, vol. 48, no. 6, pp. 2110-2120, 2012.

Contribution of individual authors

Elakhdar BENYOUSSEF : In 2015 he joined the Department of Electrical Engineering, University Kasdi Merbah of Ouargla (Algeria). His research interests are in modeling and robust control of dual three phase synchronous and induction motors and converters.

Said BARKAT : He is currently Professor of electrical engineering in university of M'sila (Algeria). His current research interests are in the field of power electronics, renewable energies, multiphase drives, and advanced control theory and applications.